

# Spectroscopic investigation of quantum confinement effects in ion implanted silicon-on-sapphire films

Rajesh Kumar\*<sup>†</sup>, H.S. Mavi and A.K. Shukla

*Department of Physics, Indian Institute of Technology Delhi, New Delhi - 110016, India*

## Abstract

Crystalline Silicon-on-Sapphire (SOS) films were implanted with boron ( $B^+$ ) and phosphorous ( $P^+$ ) ions. Different samples, prepared by varying the ion dose in the range  $10^{14}$  to  $5 \times 10^{15}$  and ion energy in the range 150-350 keV, were investigated by the Raman spectroscopy, photoluminescence (PL) spectroscopy and glancing angle x-ray diffraction (GAXRD). The Raman results from dose dependent  $B^+$  implanted samples show red-shifted and asymmetrically broadened Raman line-shape for  $B^+$  dose greater than  $10^{14}$  ions  $cm^{-2}$ . The asymmetry and red shift in the Raman line-shape is explained in terms of quantum confinement of phonons in silicon nanostructures formed as a result of ion implantation. PL spectra shows size dependent visible luminescence at  $\sim 1.9$  eV at room temperature, which confirms the presence of silicon nanostructures. Raman studies on  $P^+$  implanted samples were also done as a function of ion energy. The Raman results show an amorphous top SOS surface for sample implanted with 150 keV  $P^+$  ions of dose  $5 \times 10^{15}$  ions  $cm^{-2}$ . The nanostructures are formed when the  $P^+$  energy is increased to 350 keV by keeping the ion dose fixed. The GAXRD results show consistency with the Raman results.

## 1 Introduction

Semiconductor nanostructures (NSs) have been investigated in recent years because of their immense use in electronic and opto-electronic devices [1-3]. Silicon (Si) NSs can be prepared on a variety of

substrates (sapphire, quartz or semiconductors) for micro-electronic photonic device fabrication. The Si NSs fabricated on sapphire substrates have distinct advantages over crystalline Si (c-Si). Si-on-sapphire (SOS) is used in large-scale integrated circuitry primarily because it provides better electrical insulation to prevent stray currents in the electronic circuits. It is also used in aerospace and military applications because of its radiation resistance properties [4, 5]. Apart from its technological importance, Si NSs are also studied because of change in electronic, vibrational and optical properties as a result of quantum confinement effects.

The semiconductor structures can be fabricated using variety of techniques, which include, rf co-sputtering [6, 7], plasma decomposition of compounds [8, 9], laser-induced etching [10, 11] and continuous wave laser annealing of amorphous Si film [12, 13]. Ion implantation followed by subsequent annealing is another widely used technique for the fabrication of Si NSs [14-17]. Ion implantation technique is used because of its simplicity and compatibility with integrated circuits and of the ease of controlling particle size and density of NSs. When Si implanted  $SiO_2$  films are annealed in nitrogen or vacuum, Si NSs are formed giving rise to visible photoluminescence (PL) [18,19]. Generally in ion implantation method, NSs of desired element can be fabricated by implanting that particular ion into any matrix. Recently, Giri et al. [20, 21] have shown that Si NSs can be fabricated by implanting germanium ions into  $SiO_2$  film on Si wafer followed by annealing in an argon gas atmosphere. They showed that Si NSs are formed as a result of radiation-induced transfer of energy to Si ions and their nucleation and growth under suitable thermodynamic conditions. Further investigations of the

\*Present Address: National Institute for Nanotechnology (NINT), University of Alberta, Edmonton, Alberta, Canada.

<sup>†</sup>Corresponding Author: rajesh2@ualberta.ca

effects induced by ion-bombardment on Si films must be done. Detailed studies can be done by varying the dose and the implanted ion to look into possible Si NSs formation. One may expect a damage of the top surface as a result of ion implantation. Investigation of the damage level and possible formation of Si NSs in ion implanted SOS films will be very useful in integrating the SOS technology with microelectronics to make optical devices like Si quantum dot lasers [22, 23].

Light scattering is one of the most powerful methods for studying the structures of disordered or partially ordered solids [24, 25]. Quantitative distinction between a crystalline lattice and a lattice where some degree of disorder has been introduced can be made by Raman spectroscopy. Raman spectra of amorphous Si reveals a broad band around  $470\text{ cm}^{-1}$  [26], while the spectrum from crystalline form shows a sharp peak at  $520.5\text{ cm}^{-1}$  corresponding to the zone-centered phonon [27]. On the other hand, zone-edge phonons, which appear only in two-phonon Raman scattering, corresponds to large wave vectors and are sensitive to short-range disorder [28]. In NSs of a few nanometer size, a major modification is observed in vibrational properties due to the confinement of phonons. Raman spectroscopy is widely used technique for investigating the phonon confinement effect in NSs [29-33]. The change in the Raman line-shape is useful in determining the size, shape and size distribution of NSs, since phonon softening and widening of Raman lines are related to the size of NSs.

The purpose of this paper is to make a systematic and comparative study of structural modifications in the SOS films implanted with boron ( $\text{B}^+$ ) and phosphorous ( $\text{P}^+$ ) ions. Raman studies are done on B implanted SOS films as a function of  $\text{B}^+$  dose at constant ion energy. Asymmetrically broadened and red shifted Raman line-shapes are observed along with a hump at  $475\text{ cm}^{-1}$  for samples implanted with  $\text{B}^+$  dose higher than  $10^{14}\text{ cm}^{-2}$ . The observed Raman line-shapes are analyzed carefully using phonon confinement model (PCM). It is found that there is a formation of Si NSs in the  $\text{B}^+$  implanted samples along with an amorphous background. Raman analysis was also done on SOS samples implanted with heavier ( $\text{P}^+$ ) ions. In  $\text{P}^+$  implanted samples, the Si NSs are formed for higher ion energy (350 keV) than that for  $\text{B}^+$  implanted samples (150 keV) for same ion dose. PL and glancing angle x-ray diffraction

Table 1: Sample details and summary of Raman results. Size of Si NSs are estimated by fitting the experimental Raman data with the theoretical line-shape using phonon confinement model, Eq. (1).

Sample	Ion	Ion energy	Fluence( $\text{cm}^{-2}$ )	Raman peak	size
B1	$\text{B}^+$	150 keV	$10^{14}$	$521\text{cm}^{-1}$	-
B2	$\text{B}^+$	150 keV	$10^{15}$	$518\text{cm}^{-1}$	5 nm
B3	$\text{B}^+$	150 keV	$5 \times 10^{15}$	$517\text{cm}^{-1}$	4 nm
P1	$\text{P}^+$	150 keV	$5 \times 10^{15}$	$475\text{cm}^{-1}$	-
B3	$\text{P}^+$	350 keV	$5 \times 10^{15}$	$518\text{cm}^{-1}$	5 nm

(GAXRD) experiments are done to verify the Raman result. Furthermore, it is observed that Si NSs can be formed on crystalline SOS films by implanting an ion with an appropriate ion energy and ion dose without any post annealing treatment.

## 2 Experimental Details

Thin crystalline SOS films of thickness 500 nm are grown by a conventional CVD process. Samples B1, B2 and B3 are prepared from crystalline SOS by implanting 150 keV  $\text{B}^+$  ions with different doses of  $10^{14}$ ,  $10^{15}$  and  $5 \times 10^{15}$  ions  $\text{cm}^{-2}$  respectively. Samples P1 and P2 are prepared from crystalline SOS by implanting  $\text{P}^+$  ions with fixed fluence of  $5 \times 10^{15}$  ions  $\text{cm}^{-2}$  and energy 150 keV and 350 keV respectively. Details of all the studied samples are given in Table 1. The Raman and PL spectra were recorded by employing a spectroscopic system consisting of a SPEX-1403 double monochromator, a HAMAMATSU (R943-2) photomultiplier tube and an argon ion laser (COHERENT, INNOVA 90). The Raman spectra are recorded using an excitation photon energy  $\sim 2.41\text{ eV}$  of the argon-ion laser. The excitation photon energy of 2.6 eV was used for PL recording at room temperature. Philips X'pert, pro PW 3040 x-ray diffractometer was used for x-ray studies in glancing angle geometry with glancing angle of 2 degrees.

## 3 Results and Discussion

### 3.1 Boron implanted samples

Figure 1(a) shows the Raman spectrum of a crystalline SOS sample showing a symmetric peak at  $524\text{ cm}^{-1}$ , which is  $3.5\text{ cm}^{-1}$  blue shifted as compared to the c-Si ( $520.5\text{ cm}^{-1}$ ). The phonon hardening of 3.5

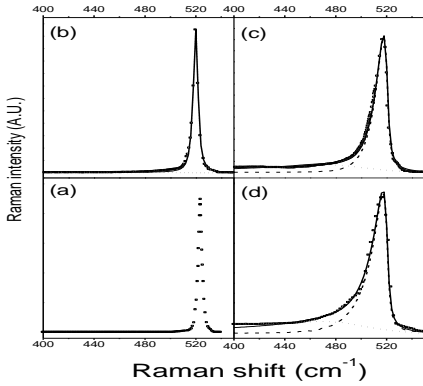


Figure 1: Raman spectra from (a) crystalline SOS and B<sup>+</sup> implanted samples prepared by implanting 150 keV B<sup>+</sup> ions with a fluence rate of (b) 10 ions cm<sup>-2</sup>, (c) 10<sup>15</sup> ions cm<sup>-2</sup> and (d) 5 x 10<sup>15</sup> ions cm<sup>-2</sup>. Discrete points are experimental data and solid line is theoretically calculated Raman line-shape. Raman signals from amorphous and nanocrystalline Si are shown by dotted and dashed lines respectively.

cm<sup>-1</sup> indicates the presence of an interfacial compressive stress of  $8.7 \times 10^9$  dyne cm<sup>-2</sup> according to Englert et al. [34]. Figures 1(b) - (d) shows the Raman spectra from samples B1, B2 and B3 respectively. The Raman peak positioned at 524 cm<sup>-1</sup> from crystalline SOS shifts to 521 cm<sup>-1</sup> when crystalline SOS is implanted with 150 keV B<sup>+</sup> ions at a rate of 10<sup>14</sup> ions cm<sup>-2</sup> as shown in Fig. 1(b). The Raman line-shape from sample B1 is symmetric with FWHM of 4.5 cm<sup>-1</sup>. The Raman peak shift from 524 cm<sup>-1</sup> to 521 cm<sup>-1</sup> may be because of relaxation in the interfacial stress due to the B<sup>+</sup> ion implantation. Because of ion implantation there is a little damage to the film surface, which gives a path for the film-interface stress to be relieved partially. This type of relaxation in the stress has also been observed on porous Si on sapphire [35]. Dubbelday et al. [35] have shown that when the SOS film is stain etched in HF: HNO<sub>3</sub> solution, crevices and cracks are formed in the film. There is a relaxation in stress as a result of increase in the porous Si layer thickness on the sapphire substrate. In our sample B1, this type of relaxation in stress may take place through the damage created by ion implantation. When the dose of B<sup>+</sup> ion is

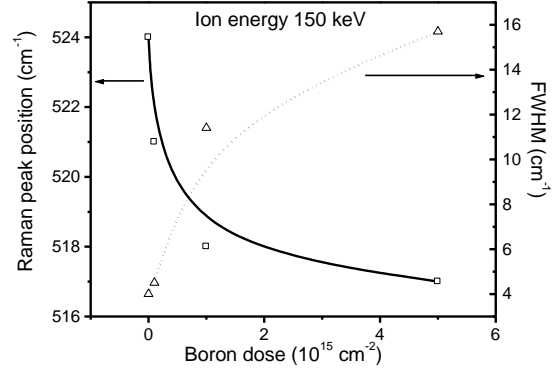


Figure 2: Variation of Raman peak position and FWHM from B<sup>+</sup> implanted samples as a function of dose with fixed ion energy of 150 keV.

increased to 10<sup>15</sup>, the Raman peak position shifts to 518 cm<sup>-1</sup> and asymmetrically broadened with FWHM of 11.5 cm<sup>-1</sup> as shown in Fig. 1(c). The Raman spectrum from sample B2 shows a hump around 475 cm<sup>-1</sup> indicating the presence of some amorphous Si background. On further increasing the dose to 5 x 10<sup>15</sup> by keeping the ion energy same (150 keV), the Raman peak downshifts further to 517 cm<sup>-1</sup> with FWHM of 15.5 cm<sup>-1</sup>. The amorphous component is also increased in sample B2 because of more amorphization due to increased B<sup>+</sup> dose.

The variation of Raman peak position and FWHM as a function of B<sup>+</sup> implantation dose is shown in Fig. 2. From the Raman spectra of B<sup>+</sup> ion implanted samples in Fig. 1, it can be seen that as the dose is increased, there is an increase in the intensity of the amorphous part (475 cm<sup>-1</sup>). The amorphization of the top SOS surface as a result of increased dose have been further verified by recording the second order Raman scattering spectra as shown in Fig. 3. Figure 3(a)-(c) show the second order Raman spectra from samples B1, B2 and B3 respectively. It is clear from Fig. 3 that the second order Raman scattering intensity diminishes with increasing B<sup>+</sup> dose on the sample. This indicates the more and more amorphization of the SOS films but complete amorphization has not taken place even at the highest B<sup>+</sup> dose of 5 x 10<sup>15</sup> ions cm<sup>-2</sup> in our case. A gradual red shift is also observed in the Raman peak position in

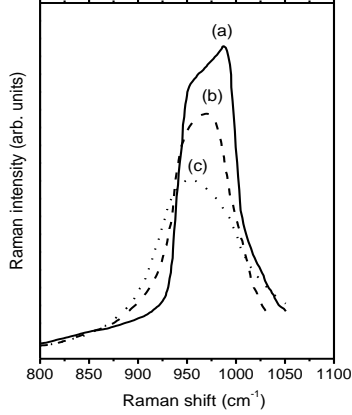


Figure 3: Second order Raman spectra from (a) sample B1, (b) sample B2 and (c) sample B3

Fig. 1. To investigate the red shift the amorphous contribution has been subtracted from the full Raman data in Figs. 1(c) and 1(d). The amorphous part is shown by dotted line and the subtracted part is shown by dashed line in Figs. 1(c) and 1(d). The Raman scattering data obtained after subtraction of the amorphous part is red shifted and asymmetric in nature. This type of behavior indicates the presence of quantum confinement effect in the samples B2 and B3. The quantum confinement of phonons is observed in the Si NSs, which have been formed in the amorphous Si matrix because of ion implantation. To get the information about the size of the Si NSs formed, the subtracted Raman spectra in Figs. 1(c) and 1(d) were analyzed within the framework of the PCM [36,37]. The PCM developed by Richter et al. [36] and Campbell et al. [37] describes the Raman line-shape of the optical phonons of low dimensional materials and has been widely reported to estimate the NSs sizes [38, 39]. Taking the phonon weighing function to be a Gaussian, the first-order Raman spectrum can be expressed as:

$$I(\omega) \propto \int_{L_1}^{L_2} N(L) \left[ \int_0^1 \frac{e^{-\frac{q^2 L^2}{4a^2}}}{[\omega - \omega(q)]^2 + \left[\frac{\Gamma}{2}\right]^2} d^3q \right] dL \quad (1)$$

where 'q' is the phonon wave vector and  $\omega(q)$  is the phonon dispersion relation for c-Si. The  $\Gamma$  is the natural line width of Raman mode and 'L' is the confinement parameter (size of the crystallite). The ' $L_1$ '

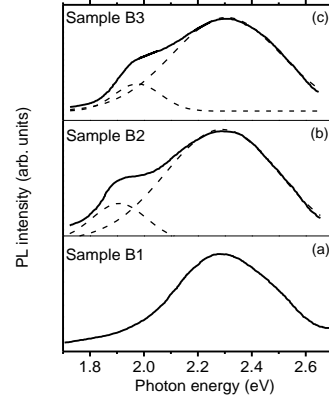


Figure 4: PL spectra from (a) sample B1, (b) sample B2 and (c) sample B3.

and ' $L_2$ ' are the minimum and maximum confinement dimensions respectively. The ' $N(L)$ ' is a Gaussian function of the form  $N(L) \cong e^{-\left(\frac{L-L_0}{\sigma}\right)^2}$  included to account for the size distribution of the NSs. Where  $L_0$  is the mean NSs size and  $\sigma$  defines the width of the distribution. The size of the Si NSs obtained from the Raman line-shape fitting is displayed in Table 1. The theoretical Raman line-shape given by Eq. (1) shows a good fit with the experimental data in Figs. 1 (c) and 1(d). The experimental data were best fitted with mean size of 5 nm for sample B2 and with 4 nm for sample B3. The decrease in the NSs size with increasing  $B^+$  dose is also consistent with the red shift of the Raman peak position.

To further confirm the formation of Si NSs, PL spectroscopy is done at room temperature. Figure 4(a)-(c) shows the PL spectra from samples B1, B2 and B3 respectively. There are two important features in Fig. 4. Firstly there is a broad PL peak centered around 2.28 eV, which is independent of the  $B^+$  ion dose. Secondly, there is an appearance of a PL band at 1.9 eV, which is absent in PL spectrum from sample B1 in Fig. 4(a). The PL peak at 1.9 eV for sample B2 shifts to 1.95 eV when  $B^+$  dose is increased from  $10^{15}$  to  $5 \times 10^{15} \text{ cm}^{-2}$ . Raman results in Table 1 show that the size of Si NSs decrease with increasing the ion dose. Therefore, the size dependent PL peak centered at 1.9-1.95 eV is attributed to the quantum confinement of electrons in Si NSs[40]. This PL peak is absent for the sample implanted with dose

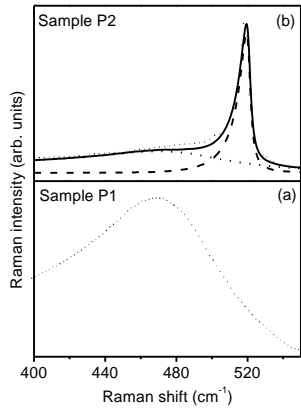


Figure 5: Raman spectra from P<sup>+</sup> ion implanted samples implanted with dose  $5 \times 10^{15}$  ions  $\text{cm}^{-2}$ . The energy of P<sup>+</sup> ions was 150 keV in (a) and 350 keV in (b). Discrete points are experimental data and the solid line is theoretically calculated Raman line-shape. Raman signals from amorphous and nanocrystalline Si are shown by dotted and dashed lines respectively in (b).

$10^{14}$   $\text{cm}^{-2}$  in Fig. 1(a). On the other hand, the PL peak at 2.28 eV doesn't show any dependence on the size (or implantation dose). This size independent PL is attributed due to the transitions between two trapped defect states as discussed by Wolkin et al. [41]. The PL results are in consonance with Raman scattering results in Figs. 1(b)-(d). On the basis of Raman and PL results from B<sup>+</sup> implanted films one can say that quantum confined effects can be observed in ion implanted SOS films.

### 3.2 Phosphorous implanted samples

To see the effect of implanted ion species on the crystalline SOS samples, Raman studies have been done on P<sup>+</sup> ion implanted samples. Figure 5(a) shows the Raman spectrum of P<sup>+</sup> ion implanted sample (sample P1) with a dose of  $5 \times 10^{15}$  and ion energy of 150 keV. One can see an amorphous structure around  $475 \text{ cm}^{-1}$  due to implantation with a heavier ion as compared to B<sup>+</sup> implanted samples. Figure 5(b) illustrates the Raman spectrum (hollow squares) from sample P2. The Raman spectrum from sample P2 shows a sharp peak at  $518 \text{ cm}^{-1}$  along with a hump

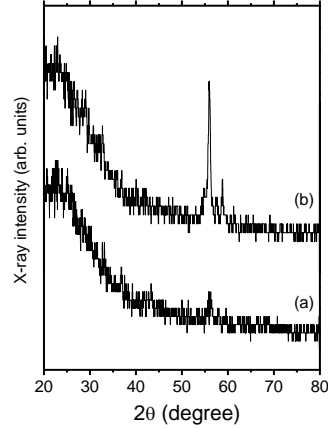


Figure 6: X-ray diffraction spectra from (a) sample P1 and (b) sample P2.

at  $475 \text{ cm}^{-1}$ . The red shifted sharp peak at  $518 \text{ cm}^{-1}$  indicates the presence of phonon confinement and needs further analysis.

The Raman result from sample P2 has been further analyzed in the same way as was done for the B<sup>+</sup> implanted Raman results in the previous section. When the amorphous part is subtracted from the full Raman data, an asymmetric Raman line-shape is obtained as shown by dashed line in Fig. 5(b). Subtracted data is fitted with Eq. (1) to get the Si NSs size. We get the best fit of experimental data for mean crystallite size of 5 nm which is less than the Bohr exciton diameter  $\sim 10 \text{ nm}$  [42]. Thus we can say that the asymmetry and red shift in the Raman line-shape in Fig. 5(b) is due to quantum confinement of phonons in the Si NSs formed due to ion implantation. It can also be observed from Fig. 5(b) that complete amorphization of the top SOS layer can be avoided by increasing the ion energy. The ions with higher energy penetrate deep into the film and the damage is less at the top surface. As a result, partial amorphous Si along with Si NSs is formed.

For further investigation of the top surface of the P<sup>+</sup> implanted sample, GAXRD studies were done. Figures 6 (a)-(b) show the GAXRD results of sample P1 and P2 respectively. The amorphous top surface of sample P1 can be seen from Fig. 6(a). Whereas, for sample P2, the GAXRD result shows a peak at  $2\theta \sim 56^\circ$  corresponding to (311) peak of Si in Fig. 6(b). Figure 6(b) suggests that the top surface of

sample P2 is not completely amorphous in nature. The GAXRD results in Fig. 6 are in consonance with Raman scattering results in Fig. 6. The Raman and GAXRD results confirm the presence of crystalline Si phase in sample P2 and complete amorphous nature of sample P1. By comparing the Raman results from B<sup>+</sup> and P<sup>+</sup> implanted samples one can say that when the crystalline SOS is implanted with P<sup>+</sup> ions at the same dose and ion energy as of B<sup>+</sup>, complete amorphization of the top SOS layer take place. To avoid the amorphization of the top layer, ions with higher energy should be used for implantation. Under this condition, quantum confinement from Si NS present in amorphous background can be seen in Raman scattering. The Si NSs present in our samples can be formed by implantation of any ion with appropriate dose and ion energy without any post annealing treatment.

## 4 Conclusions

On the whole, a comparative Raman studies on B<sup>+</sup> and P<sup>+</sup> ion implanted SOS samples are presented here. It is found that the inherent compressive stress at the interface in the crystalline SOS film can be partially relieved when 150 keV B<sup>+</sup> ions were bombarded with a fluence of 10<sup>14</sup> ions cm<sup>-2</sup>. Raman line-shapes show red-shift and asymmetry with increasing B<sup>+</sup> dose for a given ion energy. An amorphous Si contribution also appears at B<sup>+</sup> dose of 10<sup>15</sup> cm<sup>-2</sup> or higher. The top SOS surface is not completely amorphous even at the B<sup>+</sup> dose of 5x10<sup>15</sup> cm<sup>-2</sup> when implanted with B<sup>+</sup> ions. Phonon softening from 521 to 517 cm<sup>-1</sup> and increase in FWHM from 4.5 to 15.5 cm<sup>-1</sup> are observed as a function of increasing B<sup>+</sup> dose due to decrease in the size of Si NSs. The true Raman line-shape because of the quantum confinement effect alone is obtained by subtracting the amorphous contribution from the full Raman data. The deconvoluted Raman data were analyzed within the framework of PCM to obtain the size of Si NSs. Estimated value of L<sub>0</sub> using Raman line-shape fitting varies between 4-5 nm for B<sup>+</sup> implanted samples. The PL spectra of samples prepared by B<sup>+</sup> implantation on crystalline SOS show broad luminescence in the visible region. The PL from higher dose samples show two peak behavior. The 1.9 eV size dependent PL peak arises due to quantum confinement of electrons in the Si NSs fabricated by ion implantation.

Whereas, the 2.28 eV PL peak is observed due to defects in the sample.

Raman and GAXRD results show that when the crystalline SOS films are implanted with heavier ions (P<sup>+</sup> in our case) by keeping other parameters fixed, complete amorphization of the top SOS surface takes place. The amorphization of top SOS layer can be avoided if the energy of implantation is increased. The Si NCs of 5 nm sizes are formed at higher ion energy in P+ implanted sample. The dose and energy dependent Raman results from B<sup>+</sup> and P<sup>+</sup> implanted SOS samples reveal Si quantum structures, are formed if complete amorphization is avoided. The quantum confinement effect can be seen only when the dose is higher than a critical value for a given ion energy. The Si NSs in amorphous matrix can be formed by implantation of any ion with appropriate dose and ion energy without any post annealing treatment.

**Acknowledgements:** The authors are grateful to Prof. V. D. Vankar (IIT Delhi) for many useful discussions. The authors acknowledge the financial support from the Department of Science and Technology, Govt. of India under the project “Linear and nonlinear optical properties of semiconductor/metal nanoparticles for optical/electronic devices”. One of the author (R.K.) acknowledges National Research Council (NRC-Nano project) for financial assistance. Technical support from Mr. N.C. Nautiyal is also acknowledged.

## References

- [1] Duan X., Huang Y., Cui Y., Wang J., Lieber C.M., (2001) Indium phosphide nanowires as building blocks for nanoscale electronic and optoelectronic devices, *Nature* 409; 66-69.
- [2] Cui Y., Lieber C.M., (2001) Functional Nanoscale Electronic Devices Assembled Using Silicon Nanowire Building Blocks, *Science* 291; 851-853
- [3] Huang M.H., Mao S., Feick H., Yan H., Wu Y., Kind H., Weber E., Russo R., Yang P., (2001) Room-Temperature Ultraviolet Nanowire Nanolasers, *Science* 292; 1897-1899
- [4] Johnson R.A., de la Houssaye P.R., Wood M.E., Garcia G.A., Cheng C.E., Asbeck P.M., Lagnado

- I., (1997) Silicon-on-Sapphire MOSFET transmit/receive switch for L and S band transceiver application, *Electronics Lett.* 33; 1324-1326
- [5] Roig J., Flores D., Hidalgo S., Rebollo J., Millan J., (2004) Thin-film silicon-on-sapphire LDMOS structures for RF power amplifier applications, *Microelectronics J.* 35; 291-297.
- [6] Fujii M., Hayashi S. and Yamamoto K., (1990) Raman scattering from quantum dots of Ge embedded in SiO<sub>2</sub> thin films, *Appl. Phys. Lett.* 57; 2692-2694.
- [7] Mishra P. and Jain K.P., (2002) Raman, photoluminescence and optical absorption studies on nanocrystalline silicon, *Mat. Sci. & Eng. B.* 95; 202-213.
- [8] Banerjee S., Salem M.A. and Oda S., (2003) Conducting-tip atomic force microscopy for injection and probing of localized charges in silicon nanocrystals, *Appl. Phys. Lett.* 83; 3788-3790.
- [9] Oda S., (2003) NeoSilicon materials and silicon nanodevices, *Mat. Sci. & Eng. B.* 101; 19-23.
- [10] Mavi, H.S., Prusty, S., Kumar, M., Kumar, R., Shukla, A.K., Rath, S., (2006). Formation of Si and Ge quantum structures by laser-induced etching, *Phys. Stat. Sol. (a)* 203; 2444-2450.
- [11] Cheah K.W., Choy C.H., (1994) Wavelength dependence in photosynthesis of porous silicon dot *Solid State Commun.* 91; 795-797.
- [12] Mavi H.S., Shukla A.K., Abbi S.C., Jain K.P., (1989) Raman study of amorphous to microcrystalline phase transition in cw laser annealed a-Si:H films, *J. Appl. Phys.* 66; 5322-5326.
- [13] Mishra P., Jain K.P., (2000) Temperature-dependent Raman scattering studies in nanocrystalline silicon and finite-size effects, *Phys. Rev. B* 62; 14790-14795.
- [14] Shimizu-Iwayama T., Nakao S., Saitoh K., (1994) Visible photoluminescence in Si+-implanted thermal oxide films on crystalline Si, *Appl. Phys. Lett.* 65; 1814-1816.
- [15] Guha S., Pace M.D., Dunn D.N., Singer I.L., (1997) Visible light emission from Si nanocrystals grown by ion implantation and subsequent annealing, *Appl. Phys. Lett.* 70; 1207-1209.
- [16] Fischer T., Petrova-Koch V., Scheglov K., Brandt M.S., Koch F., (1996) Continuously tunable photoluminescence from Si+-implanted and thermally annealed SiO<sub>2</sub> films, *Thin Solid Films* 276; 100-103.
- [17] Wang Y.Q., Kong G.L., Chen W.D., Diao H.W., Chen C.Y., Zhang S.B., Liao X.B., (2002) Getting high-efficiency photoluminescence from Si nanocrystals in SiO<sub>2</sub> matrix, *Appl. Phys. Lett.* 81; 4174-4176.
- [18] Mutti P., Ghilotti G., Bertoni S., Bonoldi L., Cerofolini G.F., Meda L., Grill E., Guzzi M., (1995) Room-temperature visible luminescence from silicon nanocrystals in silicon implanted SiO<sub>2</sub> layers, *Appl. Phys. Lett.* 66; 851-853.
- [19] Min K. S., Seheglov K.V., Yang C. M., Atwater H., Brongersma M.L., Polman A., (1996) Defect-related versus excitonic visible light emission from ion beam synthesized Si nanocrystals in SiO<sub>2</sub>, *Appl. Phys. Lett.* 69; 2033-2035.
- [20] Giri P.K., Kesavamoorthy R., Bhattacharya S., Panigrahi B.K., Nair K.G.M., (2006) Simultaneous formation of Si and Ge nanocrystals in SiO<sub>2</sub> by one step ion implantation, *Mater. Sci. Eng. B* 128; 201-204.
- [21] Giri P.K., Kesavamoorthy R., Panigrahi B.K., Nair K.G.M., (2006) Studies on the formation of Si nanocrystals in SiO<sub>2</sub> by Ge ion implantation, *Nucl. Instr. and Meth. B* 244; 56-59.
- [22] Canham L, (2000) Gaining light from silicon, *Nature* 408; 411-412.
- [23] Wu X.L., Xue F.S., (2004) Optical transition in discrete levels of Si quantum dots, *Appl. Phys. Lett.* 84; 2808-2810.
- [24] Shukla A.K., Jain K.P., (1986) Raman scattering from ultraheavily-ion-implanted and laser-annealed silicon, *Phys. Rev. B* 34; 8950-8953.
- [25] Jain K.P., Shukla A.K., Abbi S.C., Balkanski M., (1985) Raman scattering in ultraheavily doped silicon, *Phys. Rev. B* 32; 5464-5467.

- [26] Smith J. E., Brodsky M. H., Crowder B. L., Nathan M. I., Pinczuk A., (1971) Raman Spectra of Amorphous Si and Related Tetrahedrally Bonded Semiconductors, *Phys. Rev. Lett.* 26 642-646.
- [27] Temple P.A., Hathaway C.E., (1973) Multiphonon Raman Spectrum of Silicon, *Phys. Rev. B* 7; 3685-3697.
- [28] Teicher M., Beserman R., Klein M.V., Morkoc H., (1984) Crystalline structure of mixed Ga<sub>1-x</sub>Al<sub>x</sub>As and GaP<sub>1-x</sub>As<sub>x</sub> crystals, *Phys. Rev. B* 29; 4652-4658.
- [29] Serincan U., Kartopu G., Guennes A., Finstad T.G., Turan R., Ekinei Y., Bayliss C., (2004) Characterization of Ge nanocrystals embedded in SiO<sub>2</sub> by Raman spectroscopy, *Semicond. Sci. Technol.* 19; 247-251.
- [30] Choi W.K., Ng V., Ng S.P., Thio H.H., Shen Z.X., Li W.S., (1999) Raman characterization of germanium nanocrystals in amorphous silicon oxide films synthesized by rapid thermal annealing, *J. Appl. Phys.* 86; 1398-1403.
- [31] Li B., Yu D., Zhang S., (1999) Raman spectral study of silicon nanowires, *Phys. Rev. B* 59; 1645-1648.
- [32] Wang R., Zhao G., Liu Y., Pan S., Zhang H., Yu D., Zhang Z., (2000) Raman spectral study of silicon nanowires: High-order scattering and phonon confinement effects, *Phys. Rev. B* 61; 16827-16832.
- [33] Piscanec S., Cantoro M., Ferrari A.C., Zapien J.A., Lifshitz Y., Lee S.T., Hofmann S., Robertson J., (2003) Raman spectroscopy of silicon nanowires, *Phys. Rev. B* 68; 241312 (1-6).
- [34] Englert T., Abstreiter G., Pontcharra J., (1979) 4 OPW calculations of the low-field galvanomagnetic coefficients for impurities in aluminium, *Solid Stat. Commun.* 23; 31-34.
- [35] Dubbelday W.B., Szaflarski D.M., Shimabukuro R.L., Russell S.D., Sailor M.J., (1993) Photoluminescent thin-film porous silicon on sapphire, *Appl. Phys. Lett.* 62; 1694-1696.
- [36] Richter H., Wang Z.P., Ley L., (1981) The one phonon Raman spectrum in microcrystalline silicon, *Solid State Commun.* 39; 625-629.
- [37] Campbell I.H., Fauchet P.M., (1986) The effects of microcrystal size and shape on the one phonon Raman spectra of crystalline semiconductors, *Solid State Commun.* 58; 739-741.
- [38] Ossadnik Ch., Veprek S., Gregora I., (1999) Applicability of Raman scattering for the characterization of nanocrystalline silicon, *Thin Solid Films* 337; 148-151.
- [39] Zhang S., Hou Y., Ho K., Qian B., Cia S., (1992) Raman investigation with excitation of various wavelength lasers on porous silicon, *J. Appl. Phys.* 72; 4469-4471.
- [40] Mavi H.S., Shukla A.K., Kumar R., Rath S., Joshi B., Islam S.S., (2006) Quantum confinement effects in silicon nanocrystals produced by laser-induced etching and cw laser annealing, *Semicond. Sci. Technol.* 21; 1627-1632.
- [41] Wolkin M.V., Jorne J., Fauchet P.M., Allan G., Delerue C., (1999) Electronic States and Luminescence in Porous Silicon Quantum Dots: The Role of Oxygen, *Phys. Rev. Lett.* 82; 197-200.
- [42] Cullis A. G., Canham L. T., Calcott P. D. J., (1997) The structural and luminescence properties of porous silicon, *J. Appl. Phys.* 82; 909-965.